JOURNAL OF GEOPHYSICAL RESEARCH, VOL. 112, C07023, doi:10.1029/2006JC003786, 2007

Assimilating synthetic CryoSat sea ice thickness in a coupled ice-ocean model

K. A. Lisæter,[1] G. Evensen,[1,2] and S. Laxon[3]

Received 29 June 2006; revised 22 November 2006; accepted 29 March 2007; published 20 July 2007.

[1] Simulated CryoSat ice thickness measurements have been assimilated into a coupled ice-ocean model to examine the impact in Arctic ocean prediction systems. The model system is based on the HYbrid Coordinate Ocean Model (HYCOM) and the EVP ice rheology, and the data assimilation method is the Ensemble Kalman Filter (EnKF). It is shown how ocean salinity, surface temperature, and ice concentration fields are affected by the ice thickness assimilation, and how these fields are improved relative to a free-run experiment of the model. The ice thickness assimilation primarily affects the surface properties of the ocean. By running two different assimilation experiments, it is shown how the choice of stochastic forcing is crucial to the performance of the assimilation. Specifically, it is shown how stochastic wind forcing is important to correctly describe model prediction errors, which are important for the data assimilation step. The assimilation experiments illustrate how the ice thickness observations can have a strong impact on the ice thickness estimates of the model system. The manner in which the EnKF forcing is set up is crucial, but with the correct setup, the assimilation of ice thickness measurements could have a beneficial effect on the modeled ice thickness and ocean fields.

Citation: Lisæter, K. A., G. Evensen, and S. Laxon (2007), Assimilating synthetic CryoSat sea ice thickness in a coupled ice-ocean model, *J. Geophys. Res.*, *112*, C07023, doi:10.1029/2006JC003786.

1. Introduction

[2] Sea ice is an important component of the climate. The presence of sea ice has a strong impact on the exchange of momentum, moisture and heat between the ocean and atmosphere. The high albedo of sea ice means that it affects the net short wave radiation input to the earth. Sea ice is also important for the formation of deep waters at high latitudes, and subsequently for the thermohaline circulation of the world oceans [*Aagaard and Carmack*, 1989; *Roach et al.*, 1993; *Visbeck et al.*, 1995; *Marshall and Schott*, 1999]. In addition, knowledge of the sea ice is important for operations close to the ice edge. This makes the ability to accurately forecast sea-ice parameters important for the safe operation of fisheries and offshore industries.

[3] At present, ice concentration is the most frequently observed property of sea ice. Data from airborne passive microwave sensors has given good information on the areal coverage of sea ice since the late 1970s. Information on sea ice thickness has been more sparse, with measurements by upward looking sonar mounted onboard British and US submarines serving as the most comprehensive data set, with data available from the 1950s to the 1990s. The data is, however, sparsely sampled in time and can only give ice thickness estimates along cruise tracks in the Arctic. A clear picture of the sea ice cover and its impact on climate is hard to obtain until more frequent sampling of the ice thickness is possible.

[4] The recent launch of the ICEsat satellite mission of NASA will therefore be a valuable addition to our current sea-ice observing capabilities. This satellite has shown potential for estimating sea ice freeboard, which, when compared with snow depth estimates, may be used to obtain ice thickness [*Forsberg and Skorup*, 2005]. This satellite uses laser to measure the freeboard of the sea ice, and gives an indication of sea ice thickness. A similar satellite mission, CryoSat, was launched by ESA in October 2005, but unfortunately this satellite failed before entering orbit. That mission planned to use satellite altimetry techniques to estimate freeboard of sea ice, a technique demonstrated by *Laxon et al.* [2003], and further improved for CryoSat. A replacement mission for the failed CryoSat is now scheduled for 2009.

[5] Aside from the important climate information provided by the thickness measurements, the data sets will also be important for validating sea ice models. As shown by *Rothrock et al.* [2003], there is considerable variability among different sea-ice model results presented in the literature. The ice models tend to show agreement on certain features, for instance the decline of sea ice thickness in the 1990s. On the other hand, they differ considerably in detail.

[1] Mohn-Sverdrup Center, Nansen Environmental and Remote Sensing Center, Bergen, Norway.
[2] Norsk Hydro, Oil & Energy Research Centre, Bergen, Norway.
[3] Centre for Polar Observation and Modelling, University College London, London, UK.

0148-0227/07/2006JC003786$09.00

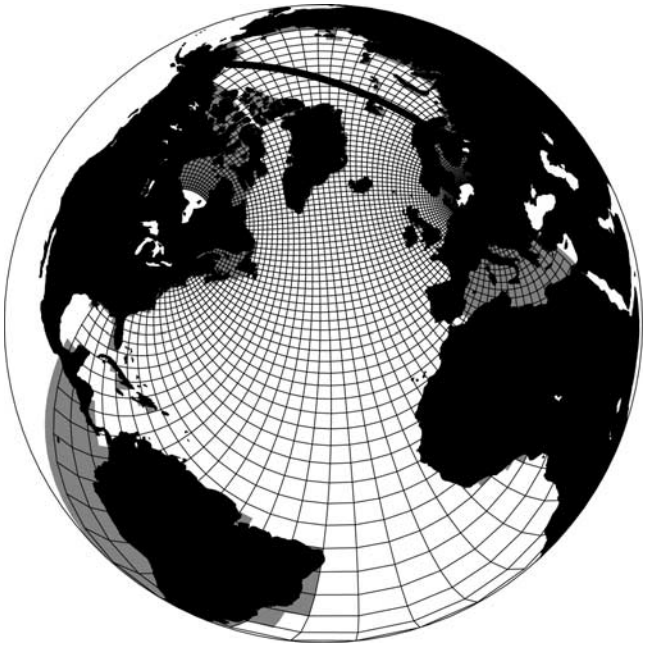

Figure 1. Illustration of the model grid. Every second grid line is shown; also shown is the location of a section referred to in the text (black line in the Arctic).

The inability of many sea ice models to properly represent annual variability has also been noted by *Laxon et al.* [2003].

[6] The assimilation of sea ice variables can be used to produce improved estimates of the sea-ice cover, as was shown by *Lisæter et al.* [2003], where sea ice concentration derived from passive microwave sensors were used. That work demonstrated how assimilation of sea-ice concentration can improve the sea-ice variables, mainly by controlling the location of the ice edge. The multivariate assimilation of sea ice concentration also affected the ice thickness, but since this happened primarily along the ice edge, the changes to the ice mass budget in the Arctic were small. In another study, *Lindsay and Zhang* [2006] found that the assimilation of ice concentration improved ice draft RMS errors and correlation between observations and modeled ice draft. However, the ice thickness bias was seen to increase after the assimilation, owing to how ice was introduced/removed in their experiment.

[7] The two studies mentioned above illustrate that it is beneficial to improve model ice thickness through data assimilation, both in uni- and multi-variate assimilation schemes. An interesting approach to improve sea-ice thickness in models is to use the information available from the sea-ice drift. The study of *Meier et al.* [2000] illustrated how sea-ice thickness could substantially change owing to the assimilation of ice drift. In another study, *Zhang et al.* [2003] assimilated sea-ice drift into their model and compared against ice thickness measurements from submarine-mounted sonars. They found that ice drift assimilation led to a reduced ice thickness bias, and an improved correlation between modeled and observed ice thickness in the Arctic.

[8] The direct assimilation of ice thickness is not yet possible on a regular basis owing to the lack of data. With future observation systems in mind, the present study will examine the potential for assimilating sea ice thickness observations in coupled sea-ice/ocean models. Using available observations, data assimilation gives an improved model estimate by combining model values and observations. Data assimilation can be used to produce historical model estimates (reanalysis), or to produce improved model forecasts. Two data assimilation experiments will be carried out using synthetic sea ice thickness estimates, which mimic error statistics from sensors which were on board the CryoSat satellite. The results from the data assimilation experiments and the impact it has on the coupled ice-ocean model should be useful for future sea-ice prediction systems.

[9] The experiments done in this work use the Ensemble Kalman Filter [*Evensen*, 1994, 2003, 2004] to assimilate synthetic sea ice thickness data into a coupled ice-ocean model. In this approach, both the state of the ocean and the ice are modified by the assimilation. We will investigate the effect of assimilating ice thickness over a 1-year period. Also of importance is the setup of the stochastic forcing in the experiments. The stochastic forcing is introduced to increase the ensemble spread, and its effect will be investigated in the different data assimilation experiments.

[10] This work is presented as follows: In section 2 the ocean/sea-ice model is presented, which is followed by a short description of the EnKF in section 3. The generation of the synthetic ice thickness fields is presented in section 4 and the setup of the experiments is described in section 5. Section 6 discusses the assimilation runs and how well they perform compared to a model run without assimilation. We also look at the impact of individual assimilation updates to the model fields, as well as the cumulative effect of the data assimilation. This section also discusses the setup of the random forcing used by the EnKF and how this affects the results. The study is summarized in section 7.

2. Model Setup

[11] The ocean model used is the HYbrid Coordinate Ocean Model (HYCOM) [*Bleck*, 2002], which is based on the Miami Coordinate Ocean Model (MICOM) [*Bleck and Smith*, 1990]. The MICOM model uses density as the vertical coordinate. The main advantage of isopycnic coordinates lies in their ability to maintain the properties of water masses which do not communicate directly with the surface mixed layer. In the interior of the ocean, mixing is believed to mainly occur along neutral surfaces [*Montgomery*, 1938], which for most situations are relatively close to isopycnic coordinate surfaces.

[12] A major change in HYCOM relative to MICOM is the introduction of hybrid coordinates, which makes it possible to mix σ-, z-, and isopycnal coordinates. This approach allows for high vertical resolution z-layers close to the surface of the ocean, and makes it easier to use advanced vertical mixing schemes in HYCOM, such as the K-Profile Parameterization [KPP; *Large et al.*, 1994] which is used in this study.

[13] The model grid has a resolution focus in the Nordic Seas with closed boundaries in the Bering Strait and the South Atlantic (see Figure 1). It was created with the conformal mapping tools of *Bentsen et al.* [1999], and has grid sizes ranging from 100 to 150 km in the Arctic. The vertical discretization consists of 22 isopycnal layers, with

densities ranging from 1021.8 to 1028.11 kg m^{-3}. Note that the lightest layers in this discretization are primarily used to describe the surface mixed layer, as they are usually too light to describe interior water masses of the ocean. The lightest layers then become the surface z layers in the hybrid coordinate formulation.

[14] The ice model uses a two-category description, where the surface is classified as ice or open water. The ice thermodynamic model uses the "0-layer" thermodynamic formulation of *Semtner* [1976], which ignores the specific heat of the ice, and a snow layer is included. The momentum exchange between the ocean and the ice is given by quadratic drag formulas. The bottom ablation of ice is given by a simple parameterization, where positive ocean heat (relative to the freezing point) is immediately used to melt the ice. As a consequence of this, the ocean temperature never deviates from the freezing point if ice is present. The ice model also calculates salinity fluxes to the ocean model when ice freezes or melts. The ice dynamics model uses the Elastic-Viscous-Plastic (EVP) ice rheology of *Hunke and Dukowicz* [1997]. The ice dynamic and thermodynamic models have been solved for the same model grid as the ocean model, shown in Figure 1.

[15] The synoptic forcing used temperature, winds, humidity, clouds, precipitation and sea level pressure from the NCEP/NCAR reanalysis [*Kalnay et al.*, 1996]. River input is modeled as a negative salinity flux. This flux is spread evenly over all ocean points within a radius of 300 km centered on the river locations. The river sources in the Arctic include the Lena, Ob, Kotuy, Dvina, Yenisei and the Mackenzie rivers [*Dümenil et al.*, 1993; *Aagaard and Carmack*, 1989]. At the surface the ocean model uses temperature and salinity relaxation toward the Generalized Digital Environmental Model (GDEM) Climatologies [*Teague et al.*, 1990], with a common relaxation time scale of 150 days. Note that if ice is present in a grid cell, no relaxation is used.

[16] The ocean fields were initialized from the GDEM Climatology, whereas the ice model was initialized with 2.5 m thick ice and 100% ice concentration wherever the GDEM climatology deviated less than 0.1°C from the freezing point of sea water. This initialization was done for the month of January, and the model was then integrated with the synoptic forcing for approximately 10 years prior to the start of the experiment. For climate studies 10 years of ocean model spin-up is probably too short, but since the focus of the experiment is on the effect of the data assimilation over a 1-year period, we deemed 10 years to be sufficient. In addition, the 10-year spin-up allows the spatial ice thickness distribution in the Arctic to evolve from the initially uniform 2.5 m ice cover to a more realistic spatial distribution, with thicker ice along the Canadian Arctic Archipelago and the northern coast of Greenland. A more detailed setup of each of the experiments is given in section 5.

3. Ensemble Kalman Filter

[17] To assimilate observational data into a model system, it is important to have a knowledge of the errors present in the model and observations. Vital statistics are the error covariance matrices of the observations and the model state. The Ensemble Kalman Filter (EnKF) [*Evensen*, 1994] uses an ensemble of model states to estimate the model error statistics.

[18] In the EnKF approach, correlation patterns will evolve according to the nonlinear evolution of the ensemble members. This comes at a cost of model resources when compared to for instance Optimal Interpolation (OI) methods [e.g., *Cooper and Haines*, 1996; *De Mey and Benkiran*, 2001; *Zhang et al.*, 2003]. The OI-methods integrate a single model state, whereas the EnKF integrates several model states in parallel, thus requiring more CPU time in total. The main advantage of the EnKF is that error statistics are calculated using different realizations of model states at the current time, rather than using error statistics specified a priori. Moreover, in multivariate data assimilation, OI methods require covariances between the assimilated variable (ice thickness) and other variables (e.g., temperature). These covariances are usually diagnosed from time-averaged statistics, or from physical reasoning, whereas in the EnKF they are derived statistically from the different model realizations. A brief explanation of the EnKF is given here; for a more thorough description of the EnKF see *Evensen* [1994, 2003, 2004] and *Burgers et al.* [1998].

[19] Let $\boldsymbol{\psi}_i^f \in \mathbb{R}^{n\times 1}$ be the n-dimensional model forecast of the ensemble member $i \in \{1, 2, \ldots, N\}$. This forecast evolves in time from the analyzed ensemble member, $\boldsymbol{\psi}_i^a$, at time t_k,

$$\boldsymbol{\psi}_i^f(t_{k+1}) = \boldsymbol{g}\left[\boldsymbol{\psi}_i^a(t_k)\right] + \boldsymbol{\beta}_i(t_k). \tag{1}$$

Here $\boldsymbol{\beta}_i \in \mathbb{R}^{n\times 1}$ is an additive stochastic error component drawn from a $\mathcal{N}(\mathbf{0}, \boldsymbol{\sigma}_\beta)$ distribution, and represents the effect of model errors on the evolution of the ensemble members. This error can be due to errors in the physical assumptions of the model and due to external errors (e.g., atmospheric forcing), in our application $\boldsymbol{\beta}_i$ is implicitly introduced by adding stochastic forcing components to the atmospheric forcing used by the coupled ice-ocean model, see section 5. The operator $\mathbf{g}$: $\mathbb{R}^{n\times 1} \rightarrow \mathbb{R}^{n\times 1}$ can, as already mentioned, be a nonlinear function of the model state.

[20] In order to infer the error evolution of the model state, knowledge is needed of the "truth." In the EnKF, the best estimate of the truth is represented by the ensemble mean state. It follows that the model state error covariance used in the EnKF is that given by the ensemble covariance. Then, at any time, an estimate of the model state error covariance matrix can be computed from the ensemble of model states as

$$\boldsymbol{P}^f \approx \boldsymbol{P}_e^f = \overline{\left(\boldsymbol{\psi}_i^f - \overline{\boldsymbol{\psi}^f}\right)\left(\boldsymbol{\psi}_i^f - \overline{\boldsymbol{\psi}^f}\right)^T}, \tag{2}$$

where $\overline{\boldsymbol{\psi}}$ is the ensemble estimated mean state, and the overbar denotes the expected value.

[21] At the time observations are available an analysis is computed. The observations $\boldsymbol{d} \in \mathbb{R}^{m\times 1}$ have an associated uncertainty $\boldsymbol{\epsilon}$, and an observation error covariance matrix $\boldsymbol{R} = \boldsymbol{\epsilon}\,\boldsymbol{\epsilon}^T$, where the observation error covariance matrix must be based on prior knowledge of the observation errors. Let $\boldsymbol{H} \in \mathbb{R}^{m\times n}$ be a linear operator that transforms the model state to

the observation space. Then the analysis update is given by the following variant of the traditional Kalman filter equation [*Jazwinski*, 1970; *Burgers et al.*, 1998]:

$$\begin{aligned}\boldsymbol{\psi}_i^a &= \boldsymbol{\psi}_i^f + \boldsymbol{P}_e^f \boldsymbol{H}^T \left(\boldsymbol{H}\boldsymbol{P}_e^f \boldsymbol{H}^T + \boldsymbol{R}\right)^{-1} \left(\boldsymbol{d}_i - \boldsymbol{H}\boldsymbol{\psi}_i^f\right) \\ &= \boldsymbol{\psi}_i^f + \boldsymbol{K}_e \left(\boldsymbol{d}_i - \boldsymbol{H}\boldsymbol{\psi}_i^f\right),\end{aligned} \tag{3}$$

where $\boldsymbol{K}_e$ is called the optimal Kalman gain. Special notice should be taken of the observation vector $\boldsymbol{d}_i$ used in equation (3); as indicated by its subscript it is different for each ensemble member. This is because the observations need to be perturbed to get an analysis error covariance matrix consistent with the original Kalman Filter. As shown by *Burgers et al.* [1998] the analysis with $\boldsymbol{d}_i$ taken from a $\mathcal{N}(\boldsymbol{d}, \boldsymbol{R})$ distribution gives the following analysis covariance matrix:

$$\boldsymbol{P}_e^a = (\boldsymbol{I} - \boldsymbol{K}_e \boldsymbol{H}) \boldsymbol{P}_e^f. \tag{4}$$

Here $\boldsymbol{I}$ is the identity matrix, and the analysis covariance matrix derived in this way is consistent with the covariance of the analysis in the Kalman Filter. Without perturbation of the original observations $\boldsymbol{d}$, the analyzed covariance would be systematically underestimated, an effect which could lead to filter divergence. By filter divergence we mean that the error estimate of the model in the EnKF is too small, and the analysis will have little impact on the model. This way significant bias can develop in the model ensemble.

[22] It should be noted that variants of the EnKF have been developed which removes the need for perturbed observations [see *Anderson*, 2001; *Whitaker and Hamill*, 2002; *Bishop et al.*, 2001; *Evensen*, 2004], but for our experiments we use the analysis method given by equation (3).

[23] In the literature, the model state errors described by the EnKF ($\boldsymbol{P}_e^f$) are frequently called EnKF estimated errors or forecast errors. In the following, we will use the term prediction error to describe this quantity.

4. Synthetic Ice Thickness Data

[24] The ice thickness data used in this study is intended to be a realistic representation of ice thickness products of the CryoSat mission. It is created using sea ice model data, which gives estimates of the ice thickness, ice concentration, surface temperature and snow thickness. The surface state is then used in a model which simulates the orbit of the CryoSat satellite, and the instrument and geophysical errors introduced by the sea ice thickness retrieval. The synthetic ice thickness data was generated for 1990, the year when the assimilation experiment takes place. It should be noted that the model used to generate the synthetic ice thickness, briefly described below, is different from the model used in the assimilation experiments.

4.1. Background Ice Thickness Data

[25] The surface state was generated from a run of a coupled sea-ice/ocean model. This model is different from the one used in the assimilation experiments, and consists of the Miami Isopycnic Coordinate Ocean Model (MICOM) [*Bleck and Smith*, 1990] coupled to a dynamic-thermodynamic sea ice model. The sea ice model uses the Viscous-Plastic rheology of *Hibler* [1979], as implemented by *Harder* [1996]. The thermodynamic module is described by *Drange and Simonsen* [1996]. Two major differences between the model used to generate synthetic ice thickness data and the one used in the assimilation experiment (section 2) are in the ocean model and the ice model. It should also be noted that the model grids are slightly different, but they both include the Arctic and the North Atlantic Ocean.

[26] The model used to generate synthetic ice thickness was run for a 40-year period, from 1958 to 1998 using NCEP forcing, and relaxation to Levitus climatologies [*Levitus et al.*, 1994; *Levitus and Boyer*, 1994]. Comparisons of the modeled fields with ice thickness from submarine sonar measurements are shown in Figure 2 for two submarine cruises done in 1990 and 1991.

4.2. Generation of Synthetic CryoSat Observations

[27] After having obtained the ice thickness estimates from the coupled ice/ocean model, the sampling pattern of CryoSat was used to obtain measurements, using the model as the ground truth. An example of the ice thickness sampled this way is shown in Figure 3. Errors were then added to the thickness estimates to simulate the errors of the CryoSat sensor. As the CryoSat satellite sensor measures the freeboard h_f, a first step is to convert model ice and snow thickness to freeboard height,

$$h_f = \frac{\rho_w - \rho_i}{\rho_w} h_i - \frac{\rho_s}{\rho_w} h_s, \tag{5}$$

where h and ρ are thickness and densities of the snow and ice (subscript i or s), and ρ_w is the density of sea water. The synthetic freeboard estimate is then calculated by adding a random error w_f to the model freeboard estimate. The random error w_f has an error variance σ_f^2, which is a function of the ice elevation error variance σ_{Eice}^2 and the ocean elevation error variance σ_{Eocn}^2,

$$\begin{aligned} h_f' &= h_f + w_f \\ \sigma_f^2 &= \sigma_{\text{Eice}}^2 + \sigma_{\text{Eocn}}^2. \end{aligned} \tag{6}$$

The error variances of ice and ocean elevation depend on formulas given by *Laxon* [2001] and *Peacock and Laxon* [2004]. These errors are functions of the surface state, depending on ice concentration, ice thickness, surface temperature and backscatter contrast between ocean and water. The errors were computed using a simulation of the CryoSat instrument and retrieval algorithms over idealized sea ice surfaces.

[28] Experience from the ERS sensors indicates that as the surface temperature reaches the melting point, the location of the surface reflection becomes ambiguous. Therefore, if the surface temperature rises above $-5°C$, the synthetic data is discarded. Furthermore, owing to a strong dependence of ice elevation error on the ice concentration, an ice concentration threshold has been introduced. If the model ice concentration is below 0.7, the synthetic data is discarded as well. We stress here that this applies only to the generation of the synthetic observations. In the experiments, any available data will be used regardless of the surface temperature or ice concentration in the model.

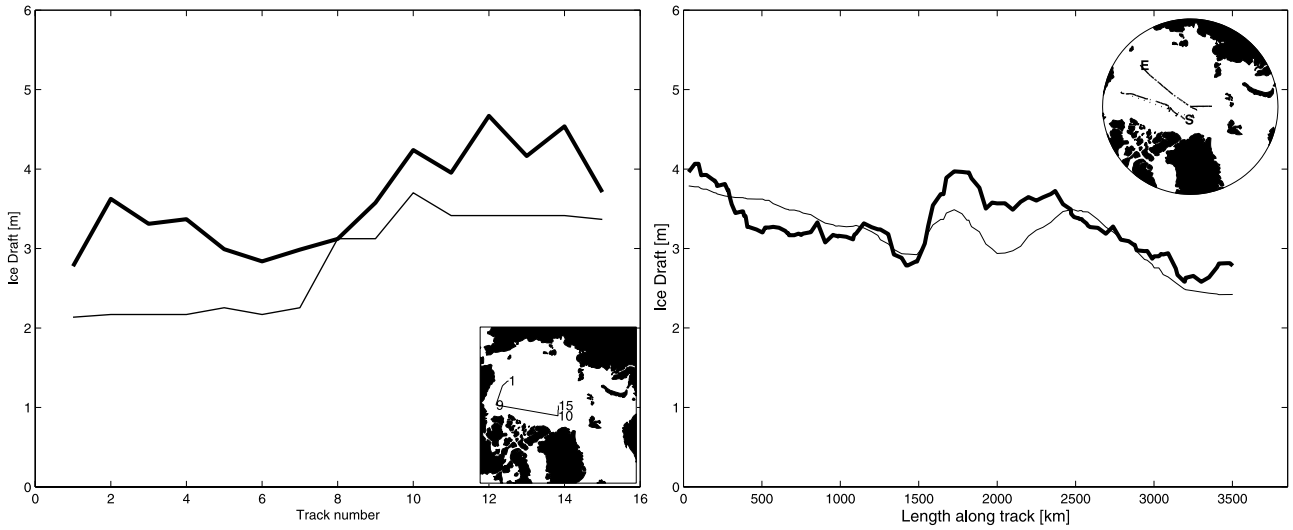

Figure 2. Comparisons between ice thickness from the model used to generate synthetic ice thickness (thin line), compared with ice thickness estimates from submarine sonars (thick line). Comparisons are for (left) 1990 and (right) 1991. Note that the x axis in the left plot denotes numbered segments along the cruise track, whereas the x axis in the right plot shows the cumulative distance along the cruise track.

[29] As the synthetic freeboard value is generated from equation (6), the synthetic ice thickness h'_i is obtained from equation (5). Likewise, the ice thickness error variance of the synthetic data can be obtained by using equations (5) and (6):

$$\sigma^2_{h'_i} = \frac{\rho_w^2\left(\sigma^2_{\mathrm{Eocn}} + \sigma^2_{\mathrm{Eice}}\right) + \rho_s^2\sigma^2_{h_s}}{(\rho_w - \rho_i)^2}, \tag{7}$$

where a snow thickness error variance has been included as well. The snow thickness error variance is based on values from *Radionov et al.* [1996] and is set to 0.0004 m^2. An example of the original model ice thickness together with the synthetic ice thickness error variance and the final synthetic ice thickness is shown in Figure 3.

[30] The original synthetic data is finally averaged over the model grid cells to give a representation which is similar to the one used in the model we assimilate data into. Note that the ice thickness error variance will be reduced when averaging the ice thickness over one grid cell. The resultant ice thickness and variance over one model grid cell becomes

$$h_i^{gc}(\Delta t) = \frac{1}{N_{gc}(\Delta t)} \sum_{j=1}^{N_{gc}(\Delta t)} h'_{i,j},$$

$$\sigma_{h_i^{gc}}(\Delta t)^2 = \frac{1}{N_{gc}(\Delta t)^2} \sum_{j=1}^{N_{gc}(\Delta t)} \sigma^2_{h'_{i,j}}, \tag{8}$$

assuming that the errors of the ice thickness measurements are uncorrelated. Here Δt is the averaging time period and $N_{gc}(\Delta t)$ is the number of measurements available in one grid cell for the averaging time period. These averaged data are to be assimilated into the model, so we drop the "gc" superscript in the following, implicitly assuming that the assimilated data are of the form in equation (8).

[31] For the experiments described in the next section we used an averaging period (Δt) of 14 days. Assuming an average ice drift of 0.1 ms^{-1}, the drift over 14 days would

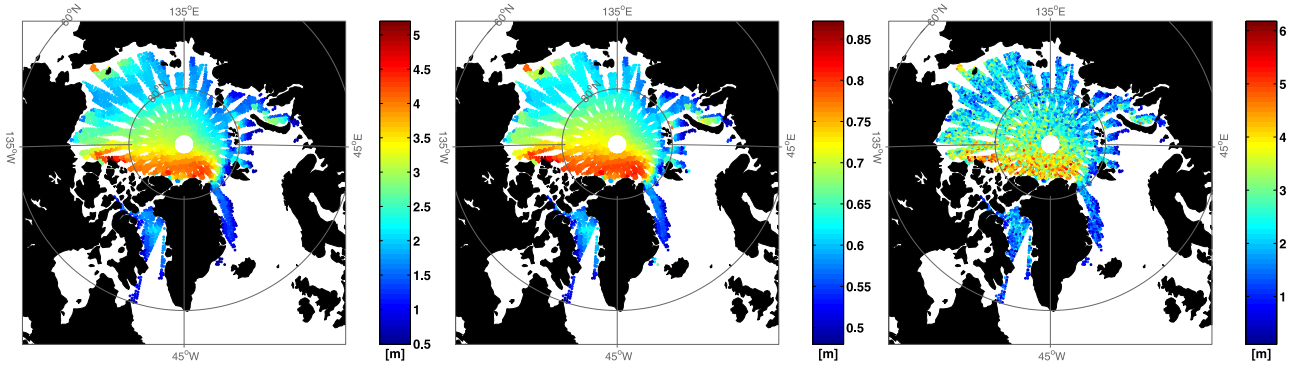

Figure 3. (left) Original ice thickness field from the model used to create the synthetic ice thickness observations. (middle) Estimated error standard deviation of the synthetic observations, calculated from equation (7). (right) Final synthetic observations, calculated by adding a random error w_{h_i} to the original observations. The figures are for Julian day 35 of 1990.

Table 1. Data Assimilation Parameters

Parameter	Description	Value
N	number of ensemble members	100
r_0	observation radius of influence	200 km
σ_c	obs. error standard deviation	equation (8)
r_c	obs. error decorrelation length scale	80 km
r_β	decorr. length for random forcing	~1000 km
Δt	averaging period/assimilation time step	14 days

become approximately 100 km, which is roughly the size of one grid cell in our model. The 14 day time period was chosen for practical purposes, while at the same time not being too long so that advective effects become too important for the averaged ice thickness. In a forecasting application, the averaging period would probably be shorter.

5. Experiment Setup

[32] The state vector ψ was chosen to include both ocean variables and ice variables as these are closely related, particularly for the mixed layer part of the ocean. For each of the 22 layers of the ocean model we included salinity, temperature, layer thickness and velocity. In addition the barotropic velocity and barotropic pressure components were included along with ice concentration, ice thickness and ice velocity from the ice model. The inclusion of variables other than ice thickness will also force an update of these variables because they can be negatively or positively correlated with ice thickness through the ensemble covariance matrix.

[33] In the analysis, sampling errors in the prediction error covariances can give rise to spurious correlation between remote points, a problem which becomes greater for smaller ensemble sizes [*Houtekamer and Mitchell*, 1998]. A common practice to counteract this is to look at the problem locally. This means that each grid cell value is updated using only observation values in a radius of influence r_0 around the grid cell [*Houtekamer and Mitchell*, 1998; *Keppenne and Rienecker*, 2002; *Brusdal et al.*, 2003], and this approach is also used here. While this limits some of the problems with spurious correlation in the prediction errors, this method may cause noisy updates by abruptly cutting off correlation functions in the ensemble. An approach which can reduce this effect is to use the method of *Houtekamer and Mitchell* [2001] which smoothly reduces these correlation functions toward zero. This method was, however, not used in this study.

[34] During the model integration there is a need to incorporate the effect of model errors on the evolution of the ensemble members. The approach used is to add pseudo-random fields, with a prescribed length scale and timescale, to the NCEP forcing fields. This procedure is a crude way of incorporating the effect of model errors $d\beta_i$ in equation (1) into the ensemble, and is similar to assuming that the dominant errors are in the forcing data. See the Appendix of *Evensen* [1994] for a description of the pseudo-random fields added to the forcing, and Table 1 for a description of the stochastic forcing component parameters used. The pseudo-random fields affect temperature and wind stress in the experiments described later (see also Table 2). Finally, it should be noted that the above procedure for generating $d\beta_i$ does not address error growth due to inaccuracies in the physical implementation of the model.

[35] The initial ensemble was generated from the 10-year spin-up of the model described in section 2. After the 10-year spin-up of a single model state, random fields were added to this model state to produce a 100 member ensemble. For each ensemble member, new ice concentration and ocean model layer thickness fields were generated by adding smooth pseudo-random fields to the original model state. All other variables of the individual ensemble members were identical to the original model state. The random fields added to the ocean model layers were vertically correlated and had a horizontal decorrelation length of ~400 km. The standard deviation of the random fields was set to 10% of the original ocean layer thickness, and the ocean layers were finally adjusted so that no barotropic waves were generated by this procedure. In a similar manner, the random fields added to the ice concentration fields had the same decorrelation length, and the standard deviation where set to 10% of the original ice concentration. This ensemble was then integrated for two more months before starting the experiments. The two month period was chosen on the basis of previous experience with the EnKF, where a relatively short ensemble spin-up was used [*Haugen and Evensen*, 2002; *Brusdal et al.*, 2003]. Ideally, a long spin-up of the ensemble is preferable, but the computing resources needed makes this unpractical.

[36] Two assimilation experiments were performed, along with a single free-run experiment for comparison. These experiments are given in Table 2. Experiments PW and SW are performed with a 100 member ensemble using the EnKF. The difference between these experiments is given in the stochastic forcing, where PW ("Perfect Wind") does not have a stochastic wind forcing component whereas experiment SW ("Stochastic Wind") has. Note that both PW and SW use a stochastic air temperature component, since a representation of β_i is needed in equation (1). Parallel to the ensemble run a free-run model was also integrated for comparison. This model was initialized from the ensemble mean at the start of the experiment, and used the standard NCEP forcing fields with no stochastic forcing components. Both EnKF experiments use the same ensemble initially.

[37] The experiments were run for a full year (January 1990 to January 1991) with the synthetic sea ice thickness data averaged and assimilated every 14 day. The data which are assimilated are first averaged for this time period as detailed in equation (8). Some of the relevant parameters for the assimilation experiment are given in Table 1.

6. Impact of the Assimilation

[38] The multivariate analysis changes the ice concentration and ice thickness of the ice model, as well as fields in

Table 2. Setup of the Stochastic Forcing in the Experiments

Experiment	Wind Stress Standard Deviation, Nm^{-2}	Air Temperature Standard Deviation, K
PW	-	2.0
SW	0.01	2.0
Free-run	-	-

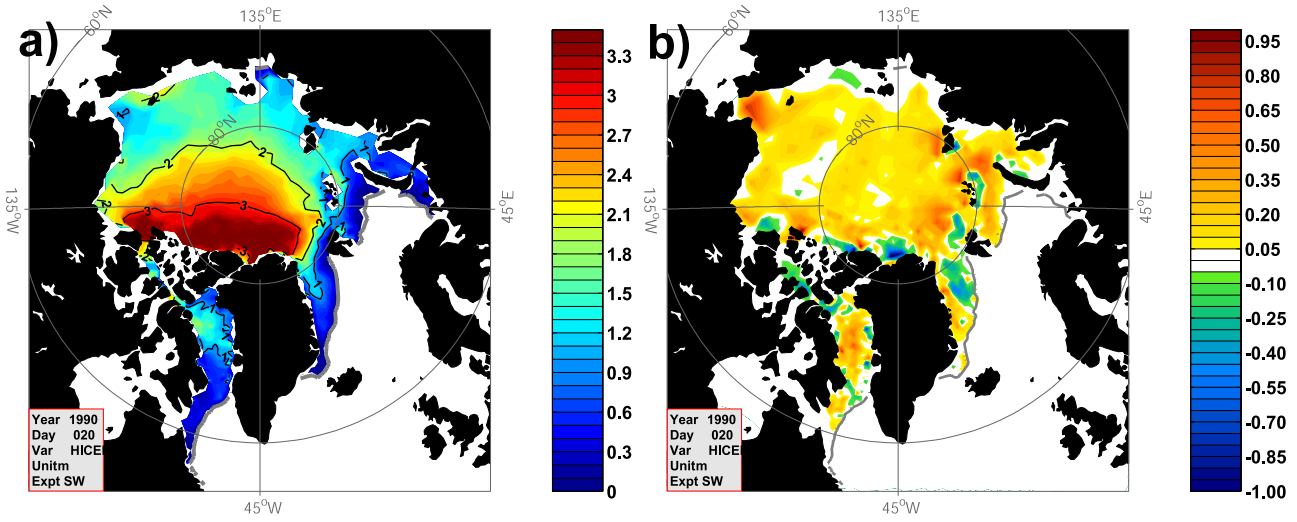

Figure 4. Example assimilation statistics from experiment SW. (a) Average ice thickness prior to the analysis on Julian day 20 in 1990. (b) Ice thickness update (analysis-forecast). Grey lines denote the 15% ice concentration contour.

the ocean model. The individual updates depend on the statistics of the observation and model prediction errors, as well as on the distance between observations and model at the location of the observations. This section shows examples of the analysis updates from the experiments, along with cumulative effects. An examination of the stochastic forcing setup is also given.

6.1. Ice Thickness

[39] Figure 4a shows the ice thickness in experiment SW on day 20, prior to the assimilation step. The ice thickness field in the model looks realistic, with a thickening of the ice cover toward the Canadian Arctic Archipelago and the northern coast of Greenland. The ice extent in the Barents Sea, Greenland Sea and the Labrador Sea is consistent with typical ice extent observed from satellite.

[40] An example of how the ice thickness assimilation changes the modeled field is shown in Figure 4b. The plot shows the ice thickness field after assimilation minus the field before assimilation. The adjustment imposed by the assimilation is complex, with intertwining regions of increased and reduced ice thickness. The end result of the assimilation at this time is an increase in the total ice mass in the Arctic.

[41] The difference between the model and the observation data is a useful quantity for the EnKF. As a tool to study this distance, we introduce the following measure:

$$\mathrm{RMS}_e(\boldsymbol{x}) = \sqrt{\mathrm{trace}\left(\overline{\boldsymbol{x}\boldsymbol{x}^T}\right)/m} \tag{9}$$

where

$$\overline{\boldsymbol{x}\boldsymbol{x}^T} = \frac{1}{\max(N-1,1)} \sum_{k=1}^{N} \boldsymbol{x}_k \boldsymbol{x}_k^T, \tag{10}$$

where $\boldsymbol{x}$ denotes a $\mathbb{R}^m$ vector, and N is the number of ensemble members. Note that $\boldsymbol{x}\,\boldsymbol{x}^T$ is an outer product, resulting in a matrix. The $N-1$ denominator is used for ensemble properties, whereas for single member experiments the denominator is 1. For an ensemble field, this measure includes effects from the ensemble variance and the mean value. For the single-member run, the measure is the standard Root Mean Square measure.

[42] The difference between observations and measurements, $\boldsymbol{d} - \boldsymbol{H}\,\psi$, is called the innovation, where $\boldsymbol{H}\,\psi$ represents the model ice thickness interpolated to the observation points. The time evolution of $\mathrm{RMS}_e(\boldsymbol{d} - \boldsymbol{H}\,\psi)$ for the assimilation experiments is shown in Figure 5a, also shown in this figure is the evolution of the RMS error for the free-run experiment. In Figure 5a there is a gap in the time series in summer, due to lack of data for that time period. As mentioned the data retrieved depends on the surface state of the ice and snow. This makes it difficult to obtain reliable freeboard measurements when the surface is close to the melting point, and the synthetic data used here reflect this.

[43] The sawtooth features in Figure 5a are the results of the sequential assimilation being performed, which draws the model solution toward the observations, thereby reducing the innovation measure. The figure shows that the assimilation experiments have the desired effect of reducing the distance between model and observations, relative to the free-run experiment. This can be seen through the individual assimilation updates, and through the cumulative effect of these updates. It should be noted that the innovation measure includes the effect of observation and model prediction errors, which both increase the RMS measure. This implies that the improvement of the ensemble mean relative to the free-run experiment is better than suggested by Figure 5a.

[44] During summer, the error of the model ensemble increases, since no synthetic data is assimilated at that time. The effect of the assimilation can, however, be seen also

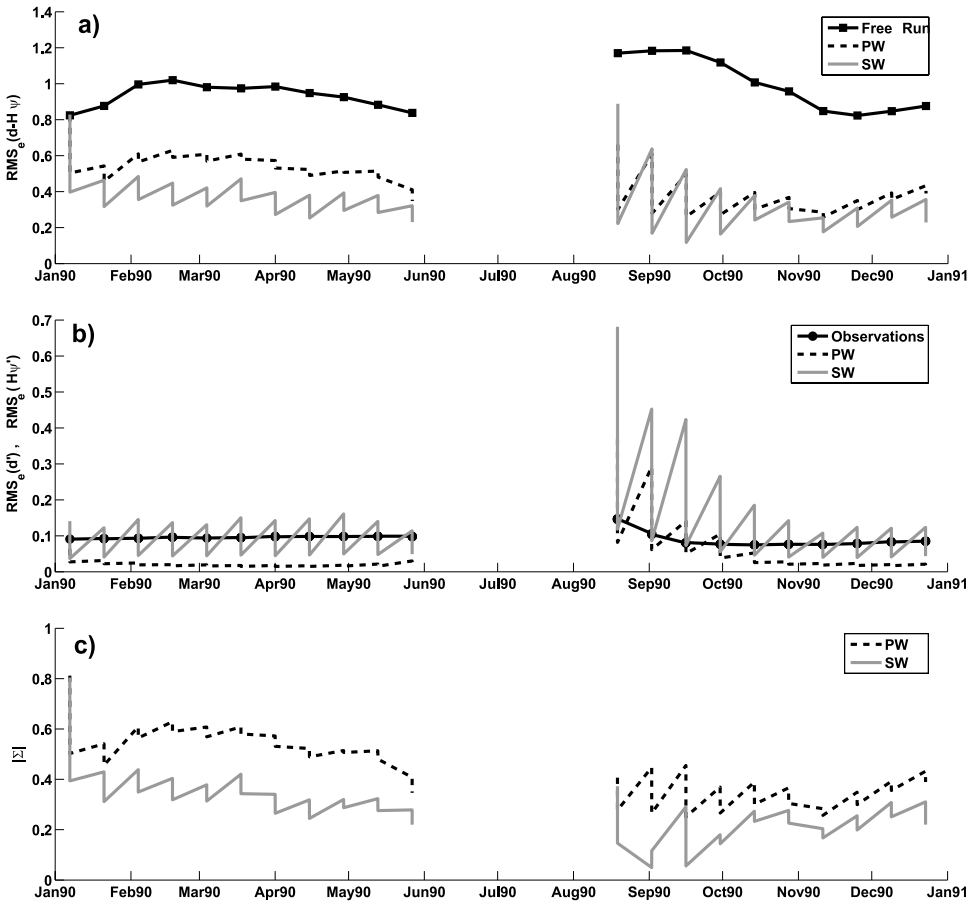

Figure 5. (a) RMS_e values of the innovation for the assimilation experiments and the RMS_e values of the innovation for the free-run experiment. (b) RMS_e for the observation errors, and the model prediction errors for the assimilation experiments. (c) Bias component $|\Sigma|$ from equation (14) for the two assimilation experiments.

after this pause in the assimilation, since the innovation RMS_e errors are smaller in the assimilation experiments than in the free-run experiment when the assimilation recommences in late summer.

[45] In assimilation experiment PW, note the relatively small assimilation updates which take place in winter (Figure 5a). The exception to this is the very first update in the experiment. After the first assimilation of ice thickness is performed in experiment PW, the remaining assimilation updates are small until the assimilation recommences in September. Weak assimilation updates are also seen at the end of the year. The cause of this can be traced back to the prediction error of the EnKF. The EnKF uses an ensemble to predict the errors, which means that the actual error covariance of the model is more likely to be underestimated in case of significant model bias.

[46] The innovation sequence can be used to provide consistency checks for the prediction error, and to investigate bias. Let the model forecast be written as

$$\psi = \psi^t + \overline{q} + \psi', \tag{11}$$

where the truth is given as ψ^t (note that by "truth" we here mean the model results which the synthetic observation are derived from). The error is decomposed into a constant (bias) part $\overline{\boldsymbol{q}}$ and an ensemble anomaly part ψ', it is the error due to the latter which the EnKF can predict. The measurements are written

$$\boldsymbol{d} = \boldsymbol{H}\psi^t + \overline{\epsilon} + \boldsymbol{d}', \tag{12}$$

where again the error ϵ has been split into a anomaly part ($\boldsymbol{d}'$) and a bias part (ϵ). This gives the following expression for the innovation covariance matrix:

$$\overline{(\boldsymbol{d} - \boldsymbol{H}\psi)(\boldsymbol{d} - \boldsymbol{H}\psi)^T} = \boldsymbol{R} + \boldsymbol{H}\boldsymbol{P}^f\boldsymbol{H}^T + (\overline{\epsilon} - \boldsymbol{H}\overline{\boldsymbol{q}})(\overline{\epsilon} - \boldsymbol{H}\overline{\boldsymbol{q}})^T, \tag{13}$$

where model and measurement anomalies are assumed to be uncorrelated. Also note that it is the difference in bias between measurements and model which contribute to the innovation covariance matrix. The measure $RMS_e(\boldsymbol{d} - \boldsymbol{H}\psi)$ can be written

$$[\mathrm{RMS}_e(\boldsymbol{d} - \boldsymbol{H}\psi)]^2 = [\mathrm{RMS}_e(\boldsymbol{d}')]^2 + [\mathrm{RMS}_e(\boldsymbol{H}\psi')]^2 + [\Sigma(\overline{\epsilon}, \overline{\boldsymbol{q}})]^2, \tag{14}$$

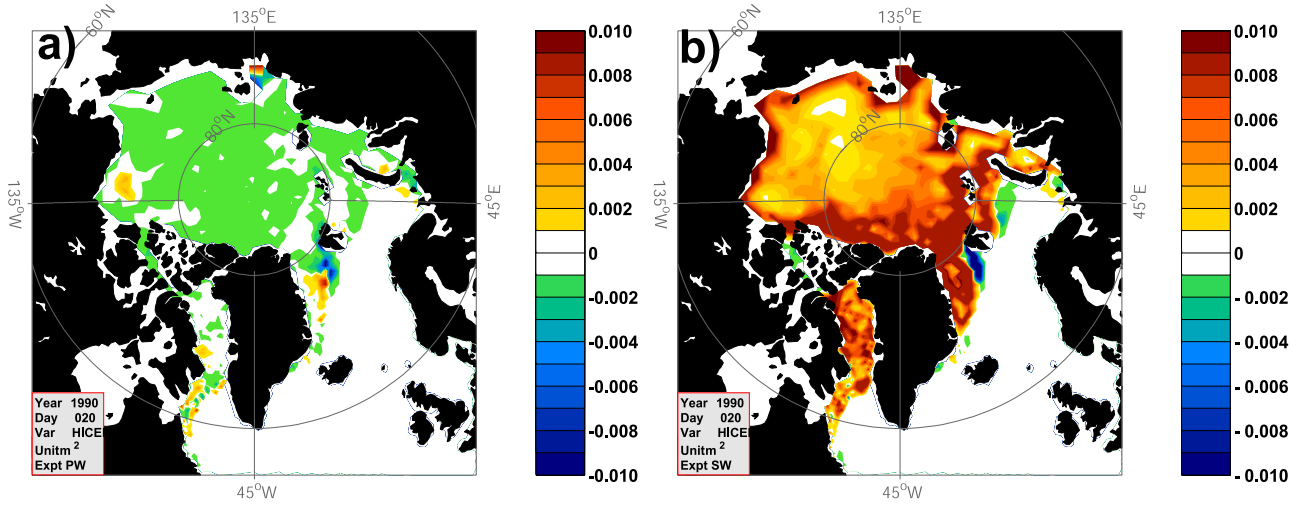

Figure 6. Growth of prediction error between two assimilation steps. The difference shows the prediction error variance on day 20 in 1990 minus the prediction error variance on day 6 in 1990. Shown are results for (a) experiment PW and (b) experiment SW.

where the last component is the effect of model and measurement bias. The size of this bias component can now be estimated from equation (14). Figure 5b shows the components due to observation errors and model prediction errors, $\mathrm{RMS}_e(\boldsymbol{d}')$ and $\mathrm{RMS}_e(\boldsymbol{H}\,\boldsymbol{\psi}')$, which can be calculated directly from the ensemble. Figure 5c shows the component due to Bias, $|\boldsymbol{\Sigma}(\bar{\boldsymbol{\epsilon}}, \bar{\boldsymbol{q}})|$.

[47] In data assimilation schemes it is frequently assumed that there is no bias in model and measurements, and this assumption is also used by the Ensemble Kalman Filter. Figure 5c shows that the bias component $|\boldsymbol{\Sigma}|$ is usually of the same magnitude as the measurement and model prediction errors. Proper treatment of bias is still a big challenge, and is out of the scope of this paper. Here we mainly note that the bias problem is larger in the experiment without stochastic wind forcing, experiment PW. Also note that the bias component is usually reduced by the assimilation, and that this reduction is stronger in the experiment with stochastic wind forcing, experiment SW. The reason for this is connected to underestimation of model prediction errors.

[48] The model prediction errors are of high importance when the assimilation is performed. Although bias is a problem, it becomes a much larger problem if the model prediction errors are severely underestimated. Figure 5b shows the prediction errors along with the measurement errors, and it clearly illustrates how the prediction errors in experiment PW are much lower than the prediction errors of experiment SW, also they are much lower than the observation errors.

[49] To illustrate how too low prediction errors affect the data assimilation, it is useful to consider the scalar version of equation (3). Let ψ_i^f be the forecasted scalar (e.g., ice thickness), let d_i be the observation of this scalar, and let P_e^f and R be the predicted error variance and observation error variance, respectively. We then have

$$\psi_i^a = \psi_i^f + \frac{P_e^f}{P_e^f + R}\left(d_i - \psi_i^f\right) = \frac{P_e^f}{P_e^f + R} d_i + \frac{R}{P_e^f + R}\psi_i^f, \quad (15)$$

which shows that for low prediction errors P_e^f, the data assimilation would give very low weight to the value d_i. In such cases the analysis ψ_i^a is close to the forecast estimate ψ_i^f.

[50] The lowest prediction errors in experiment PW are found in the beginning of the experiment, January–June 1990, and they are also found at the end of the experiment, October–December 1990. Roughly speaking, the low prediction errors coincide with freezing conditions in the central Arctic. For the current setup of the model, the results of experiment PW show that the ensemble in this case is not suited to describe the prediction errors. This is primarily due to insufficient prediction error growth between the assimilation time steps. In fact, for many of the time intervals between the assimilations, one can see a decrease in the estimated error of experiment PW (Figure 5b).

[51] An example of the low prediction error growth is shown in Figure 6a, which gives the growth after the analysis on day 6 in 1990 until day 20 in 1990, prior to the next analysis. The figure shows that for the setup in experiment PW there is a reduction in prediction error for almost the entire Arctic Basin. This behavior should be contrasted to the prediction error growth in experiment SW (Figure 6b), where the inclusion of a stochastic wind forcing component leads to a increased prediction error in the model ensemble. The difference in error growth between assimilation steps is crucial for the improved results of experiment SW when compared to experiment PW. The main reason for the differences in ice thickness is wind-forced differences in local divergence and convergence of sea ice, which modifies its thickness through sea-ice ridging. In addition, local divergence of sea ice creates open water in winter, which greatly increases heat fluxes to the atmosphere, and increases ice production.

[52] As illustrated here, maintaining model prediction errors depend greatly on the formulation of the stochastic forcing of the model ensemble used here. It should be mentioned that there are also other approaches for main-

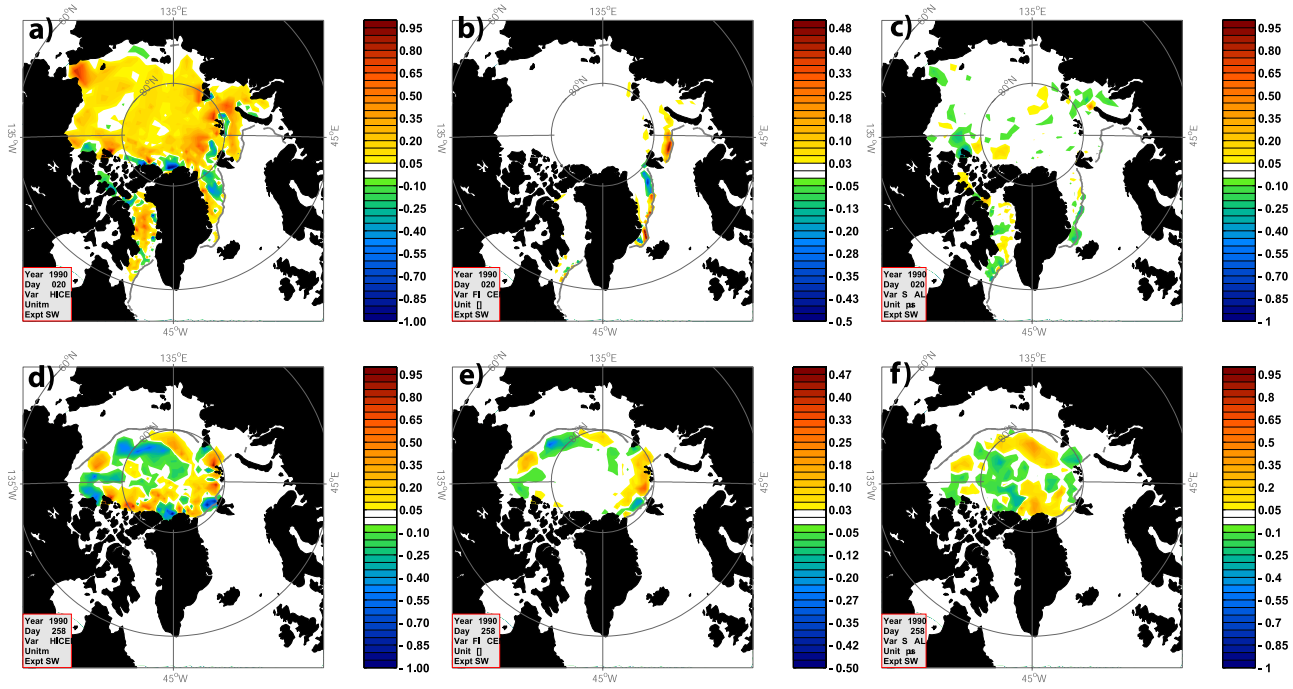

Figure 7. (left) Effect of the assimilation on ice thickness, (middle) ice concentration, and (right) sea surface salinity for experiment PW. Shown are updates (after-before assimilation) for (top) day 20 and (bottom) day 258.

taining variance of the model ensemble [see, e.g., *Pham*, 2001; *Hamill and Whitaker*, 2005].

6.2. Effects on Other Variables, and Long-Term Effects

6.2.1. Surface Variables

[53] As the observed variable, ice thickness, is updated in the assimilation, so will other variables be updated through their covariances with the ice thickness fields. An example from experiment SW, showing surface salinity, temperature and ice concentration updates, along with ice thickness updates is shown in Figure 7 for two different times, one in winter (day 20, 1990) and one in late summer (day 258, 1990). From the different plots the assimilation of the ice thickness data has a visible effect on the other variables in the ice and ocean model.

[54] The wintertime assimilation update shows how the ice thickness assimilation mainly affects the ice concentration close to the ice edge. Within the ice edge, there is very little effect of the assimilation on the ice concentration fields (Figure 7b). This can be traced back to a very low ice concentration variance within the ice edge in winter, due to ice covering close to 100% of the surface. This can also be seen in ice concentration derived from passive microwave sensors, and from Radarsat estimates [*Kwok*, 2002]. No ice concentration variance leads to no ice concentration update when assimilating ice thickness. In summer, this effect still remains, but to a lesser degree than in winter. Although the central ice pack remains largely unaffected by the assimilation, there is now a broader band along the ice edge which is affected by the assimilation when compared to the wintertime situation (Figure 7e). This wider region of large ice concentration updates can be attributed to a wider region of melt along the ice edge.

[55] Sea surface salinity is affected by the assimilation of ice thickness, and there is an impact both in winter and in summer, generally for the entire ice pack. In winter the updates of sea surface salinity (Figure 7c) do not have a clear connection to the updates in ice thickness. We speculate that this may be due to lead opening/closing over short timescales, which leads to a more saline ocean, but may have a small impact on ice thickness. In summer, however, the analysis update in surface salinity (Figure 7f) often has similar spatial patterns to the analysis update in ice thickness. This is related to the ensemble behavior at this time of year, when the covariance between sea surface salinity and ice thickness is mostly positive owing to vertical ice melt.

[56] Sea surface temperature (not shown) is, much in the same way as ice concentration, to a large extent unaffected by the ice thickness assimilation in the central ice pack. The reason for this is that the model temperature at the sea surface is constrained to the freezing point when ice is present. Therefore, within the central ice pack, there is very little variation in sea surface temperature, while close to the ice edge the variation is larger. This holds both in winter and in summer. Note, however, that changes to sea surface temperature is important when the assimilation introduces ice in ice-free regions. In these cases the temperature is reduced by the assimilation, which prevents immediate melting of the newly introduced ice.

[57] The ensemble updates are related to the underlying statistics of the ensemble which again are related to dynamical mechanisms in the model ensemble. For instance, freezing anomalies in the ensemble can lead to a positive correlation between ice thickness and sea surface salinity, as the ice expels brine to the underlying ocean. On the other hand, ice dynamics can change this, for instance can local

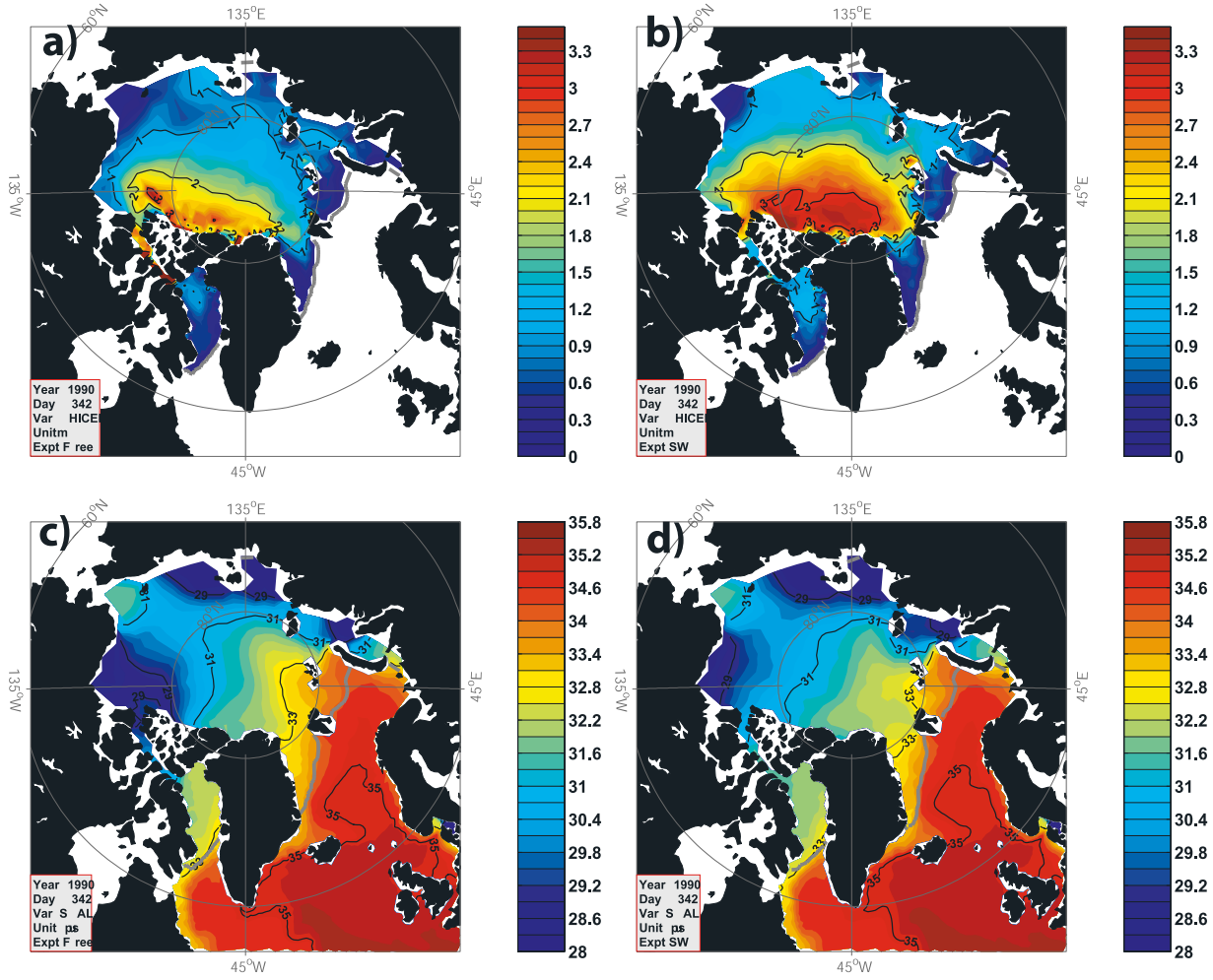

Figure 8. Sample ice thickness and surface salinity at the end of the experiment, day 342 in 1990. Grey lines denote the ice edge. (top) Ice thickness and (bottom) sea surface salinity. (left) Free-run experiment and (right) experiment SW.

divergence lead to a negative correlation between ice thickness and sea surface salinity. This can happen because ice divergence transports thick ice out of a region, which leads to increasing areas of open water being exposed to freezing conditions, which again increases the ice production while producing thin ice. The net effect is a reduced ice thickness in the region along with an increase in sea surface salinity, leading to negative correlation. The inability to precisely anticipate these and similar effects is one of the reasons for using methods such as the Ensemble Kalman Filter.

6.2.2. Cumulative Effects

[58] The long-term effects of the assimilation can be seen when comparing the model fields of experiment SW with those of the free-run experiment. The ice thickness and surface salinity fields for the free-run and SW experiments are shown in Figure 8 near the end of the experiments, at day 342. The result of the assimilation is an ice thickness which is closer to the ice thickness fields which the synthetic observations are based upon (see Figure 8b versus Figure 8a). The assimilation experiment shows an ice cover which is thicker, especially in the vicinity of the Canadian Arctic Archipelago, and the northern coast of Greenland.

[59] The differences in the ice thickness fields are not reflected in the ice concentration fields. Both experiments show an ice concentration close to unity within the ice pack (not shown), as is expected at this time of year. The location of the ice edge is also very similar in the free-run and assimilation experiments at this time of year (see grey lines in Figures 8a and 8b).

[60] Although the ice concentration fields are similar in Figures 8a and 8b, it should be noted that the ice concentration fields look different in summer. The assimilation experiments have a larger sea ice extent in summer than the free-run experiment (Figure 9). This is partly the reason for the very high ice thickness RMS errors found in summer in the free-run experiment.

[61] The surface salinity fields also show a clear effect of the ice thickness assimilation, most noticeably in the central Arctic Ocean (Figures 8c and 8d). Knowing that sea ice has a lower salinity (~6 psu) than Arctic sea water (~33 psu), an increased sea ice mass means that the underlying ocean should be saltier if more ice freezes. This expected development of the ocean salinity can be found in the surface salinity fields.

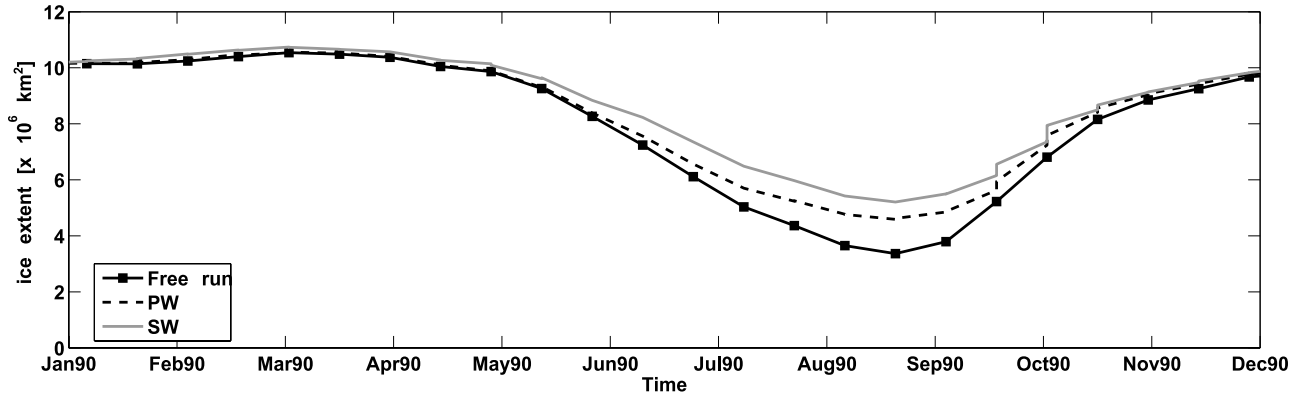

Figure 9. Ice extent from the free-run (solid line with squares), the PW (dashed black line), and SW experiments (solid gray line).

[62] The free-run experiment, having lower ice mass, shows generally lower salinity values in the central Arctic Ocean than what is seen in assimilation experiment SW. This is, again, especially pronounced north of Greenland and the Canadian Arctic Archipelago, where more ice mass is located in the assimilation experiment (note for instance the location of the 29 and 31 psu isohaline north of the Canadian Arctic Archipelago).

[63] On the other hand, the sea surface salinity can be seen to be lower between Svalbard and Frantz Josefs Land. The reason for this is due to ice exported from the Arctic into the Barents Sea, as the thick ice melts in the Barents Sea the assimilation experiments show a lower sea surface salinity here. Similarly the Fram Strait region has a lower salinity in the assimilation experiment as well.

[64] It is interesting to note that the meridional overturning and the meridional heat transport (not shown) changes very little in the assimilation experiments, relative to the free-run experiment. It is expected that the export of thicker ice into the Greenland Sea would modify deep water formation there, and so could affect the overturning. On the other hand, the time frame of our experiment (one year) may be to short to see the effect of the added freshwater flux into the Greenland Sea.

6.2.3. Pan-Arctic Section Results

[65] The assimilation also affects the deeper layers of the ocean model, but to a much smaller degree than at the surface. The temperature and salinity of the deep model layers remain virtually unchanged, and the main changes to these variables occur in the mixed layer of the ocean.

[66] In hybrid and isopycnal models the layer interfaces can move up or down in the water column as a result of mass fluxes, so the assimilation can influence the interfaces between model layers. The main changes in the deep ocean are in the thickness of the ocean layers. Illustrations of the changes to the ocean layers are shown in Figure 10b for day 34 and in Figure 10a for day 314, along with the changes in ice thickness at those times. The black line denotes the situation before the assimilation, and the grey line denotes the situation after the assimilation. The section used is depicted in Figure 1. The section goes from the northern coast of Norway, through the Barents Sea and across the Arctic Ocean.

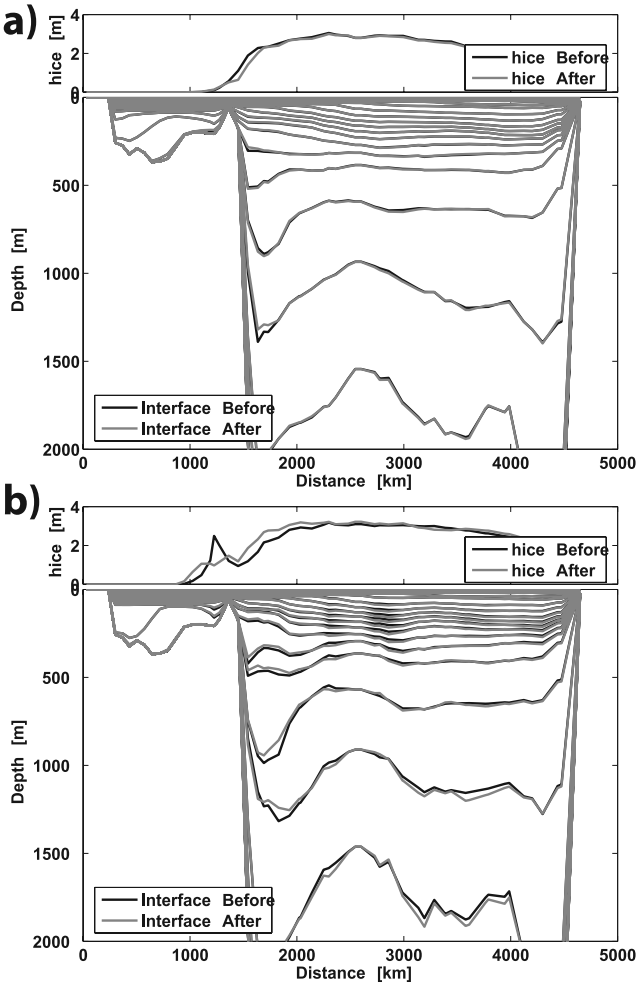

Figure 10. Interfaces between layers of the ocean model along with ice thickness, for the section in Figure 1. The plots show the ice thickness and layer interfaces before (black) and after (grey) the assimilation in experiment SW. (a) Situation on Julian day 314 in 1990. (b) Situation on Julian day 34 in 1990.

[67] The experiments show that the changes to the ocean layer interfaces are largest in the beginning of the experiment, for instance on day 34, depicted in Figure 10b. Toward the end of the experiment, the assimilation of ice thickness has very little impact on the deeper ocean layers, although they can give relatively large changes to non-z-level layers closer to the surface.

[68] It is hard to make any suggestions to physical mechanisms which lead to the covariance between layer thickness and ice thickness in these plots. For instance, on day 34 the increased ice thickness after the assimilation seems to result in lifting of the isopycnals in the waters of Atlantic origin north of the Barents Sea. On the other hand, on day 314 there is the opposite effect where a decreased ice thickness also leads to a slight lifting of the isopycnals. It is possible that large-scale effects makes it difficult to connect local changes to the ice thickness to local changes to the isopycnic layers. For instance, the correlations in the ensemble could be due to large-scale circulation changes which in turn change the isopycnal layers in the Arctic. This can make it difficult to connect local changes to ice thickness (e.g., north of the Barents Sea) to local changes in the distribution of the isopycnals. Another effect which can make the interpretation difficult are sampling errors, which can lead to spurious correlations in the ensemble.

[69] Overall, the changes in the deep ocean are small, which one might expect for a 1-year experiment. In order to properly assess any changes to the deep ocean a longer experiment may be needed.

7. Summary and Conclusions

[70] The synthetic ice thickness assimilation has been demonstrated in a coupled ice-ocean model, and shown to have an impact on both the ocean and sea-ice variables. The impact changes throughout the season, depending on the evolution of the ensemble, and the associated prediction errors. For instance, the prediction error depend on the location of the ice edge and it also depends on the sea-ice albedo feedback in summer.

[71] The cumulative effect of the ice thickness assimilation was demonstrated. The ice thickness fields in the assimilation experiment are closer to the ice thickness fields which the synthetic observations are derived from, when compared to the free-run experiment. The effect of the assimilation on the sea surface salinity in the Arctic also looks realistic, when one considers the change in ice thickness. The thicker ice in the assimilation experiments leads to increased salinity in much of the central Arctic, as expected from salinity conservation of the ice-ocean system. There is also a reduced salinity in regions of the Barents Sea and the Fram Strait, due to the export of thicker ice in the assimilation experiment, and subsequent melting in those regions.

[72] The experiments also illustrate how the EnKF is sensitive to the stochastic forcing, which is used to produce spread in the ensemble. When the EnKF was run with stochastic temperature forcing only, the model ensemble underestimates the prediction error of the ensemble. Applying an additional random wind forcing component leads to increased prediction error estimates, and generally better results.

[73] The model experiments are done on a coarse model grid, for a practical sea-ice forecasting system a higher resolution is likely to be used. We can only speculate on how this would affect our results, but as lower spatial scales are resolved, more internal variability should be present. This could make the system less dependent on the random forcing which has been used here. However, as for any assimilation method, some sensitivity experiments are needed to find a good setup for such a system.

[74] The ice thickness estimates used here are synthetic, and the final results from the CryoSat 2 mission may be different. The sampling pattern used when creating the synthetic data set should be realistic, while the error characteristics of the sensor itself is uncertain. The errors should, however, represent our best knowledge of the characteristics of the CryoSat sensor. These will be refined during the development phase of CryoSat2. Also, looking at the ice thickness values used to create the ''CryoSat'' data, they compare favorably to measurements based on ULS data, see Figure 2.

[75] Irrespective of the validity of the synthetic data set which has been used here, the experiments show that the assimilation of ice thickness is able to correct the difference between the model and the synthetic ice thickness. We believe that this will still hold when the synthetic observations used here are replaced with actual ice thickness estimates from a CryoSat mission.

[76] Assimilation of sea-ice concentration in a coupled ice-ocean model was demonstrated by *Lisæter et al.* [2003]. In that study it was shown how assimilation could provide improved estimates of sea-ice concentration. That study also showed that the sea-ice concentration assimilation did have an impact on sea-ice thickness. However, this mainly occurred along the sea-ice edge, the thickness within the ice pack was more or less unaffected. The sea ice thickness will therefore provide a complementary data set for the purpose of assimilating data into sea-ice models.

[77] The availability of continuous sea-ice thickness measurements makes the ice observing missions from ESA and NASA valuable additions to our space-observing capabilities. The experiments done in this study show how ice models can benefit from assimilating ice thickness measurements, and that efforts should be continued to further develop assimilation techniques in preparation for missions like CryoSat2. In addition, further exploration of the errors in altimeter retrievals should be performed, since these are critical for data assimilation schemes.

[78] **Acknowledgments.** Knut Lisæter has been funded by the Norwegian Research Council Ph.D. Fellowship program, under contract number 134313/432. The authors have also benefited from the support of European Space Agency contracts 13971/00/NL/DC and 14992/01/NL/MM, as well as the EC FP-5 TOPAZ project (EVK3-CT2000-00032) and the EC MERSEA project (SIP3-CT-2003-502885). The Research Council of Norway (Programme for Supercomputing) has supported the model experiments through a grant of computing time. Frank Mohn is also acknowledged for a private endowment to the Mohn-Sverdrup Center. The authors would finally like to thank three anonymous reviewers for their careful reading of the manuscript.

References

Aagaard, K., and E. C. Carmack (1989), The role of sea ice and other fresh water in the arctic circulation, *J. Geophys. Res.*, *94*(C10), 14,485–14,498.

Anderson, J. L. (2001), An ensemble adjustment Kalman filter for data assimilation, *Mon. Weather Rev.*, *129*, 2884–2903.

Bentsen, M., G. Evensen, H. Drange, and A. D. Jenkins (1999), Coordinate transform on a sphere using conformal mapping, *Mon. Weather Rev.*, *127*, 2733–2740.

Bishop, C. H., B. J. Etherton, and S. Majumdar (2001), Adaptive sampling with the Ensemble Transform Kalman Filter. part 1: Theoretical aspects, *Mon. Weather Rev.*, *127*, 420–436.

Bleck, R. (2002), An oceanic circulation model framed in hybrid isopycnic–Cartesian coordinates, *Ocean Modell.*, *1*, 55–88.

Bleck, R., and L. Smith (1990), A wind-driven isopycnic coordinate model of the north and equatorial Atlantic Ocean. 1. Model development and supporting experiments, *J. Phys. Oceanogr.*, *95*, 3273–3285.

Brusdal, K., J. M. Brankart, G. Halberstadt, G. Evensen, P. Brasseur, P. J. van Leeuwen, E. Dombrowsky, and J. Verron (2003), A demonstration of ensemble-based assimilation methods with a layered OGCM from the perspective of operational ocean forecasting systems, *J. Mar. Syst.*, *40–41*, 253–289.

Burgers, G., P. J. van Leeuwen, and G. Evensen (1998), Analysis scheme in the Ensemble Kalman Filter, *Mon. Weather Rev.*, *126*, 1719–1724.

Cooper, M., and K. Haines (1996), Altimetric assimilation with water property conservation, *J. Geophys. Res.*, *101*(C1), 1059–1077.

De Mey, P., and M. Benkiran (2001), A multivariate reduced-order optimal interpolation method and its application to the Mediterranean basin-scale circulation, in *Ocean Forecasting, Conceptual Basis and Applications*, edited by N. Pinardi and J. D. Woods, pp. 281–306, Springer, New York.

Drange, H., and K. Simonsen (1996), Formulation of air-sea fluxes in ESOP2 version of MICOM, *Tech. Rep. 125*, Nansen Environ. and Remote Sens. Cent., Bergen, Norway.

Dümenil, L., K. Isele, H. J. Liebscher, U. Schröder, and K. Wilke (1993), Discharge data from 50 selected rivers for GCM validation, *Tech. Rep. 100*, Max Planck Inst. für Meteorol., Hamburg, Germany.

Evensen, G. (1994), Sequential data assimilation with a nonlinear quasi-geostrophic model using Monte Carlo methods to forecast error statistics, *J. Geophys. Res.*, *99*(C5), 10,143–10,162.

Evensen, G. (2003), The Ensemble Kalman Filter: Theoretical formulation and practical implementation, *Ocean Dyn.*, *53*(4), 343–367.

Evensen, G. (2004), Sampling strategies and square root analysis schemes for the EnKF, *Ocean Dyn.*, *54*(6), 539–560.

Forsberg, R., and H. Skorup (2005), Arctic Ocean gravity, geoid and sea-ice freeboard heights from ICESat and GRACE, *Geophys. Res. Lett.*, *32*(21), L21502, doi:10.1029/2005GL023711.

Hamill, T. M., and J. S. Whitaker (2005), Accounting for the error due to unresolved scales in ensemble data assimilation: A comparison of different approaches, *Mon. Weather Rev.*, *133*, 3132–3147.

Harder, M. (1996), Dynamik, rauhigkeit und alter des meereises in der arktis, Ph.D. thesis, Alfred-Wegner-Inst. für Polar- und Meereisforsch., Bremerhaven, Germany.

Haugen, V. E. J., and G. Evensen (2002), Assimilation of SLA and SST data into an OGCM for the Indian Ocean, *Ocean Dyn.*, *52*, 133–151.

Hibler, W. D., III (1979), A dynamic thermodynamic sea ice model, *J. Phys. Oceanogr.*, *9*, 815–846.

Houtekamer, P. L., and H. L. Mitchell (1998), Data assimilation using an ensemble Kalman filter technique, *Mon. Weather Rev.*, *126*, 796–811.

Houtekamer, P. L., and H. L. Mitchell (2001), A sequential Ensemble Kalman Filter for atmospheric data assimilation, *Mon. Weather Rev.*, *129*, 123–137.

Hunke, E. C., and J. K. Dukowicz (1997), An elastic-viscous-plastic model for sea ice dynamics, *J. Phys. Oceanogr.*, *27*, 1849–1867.

Jazwinski, A. H. (1970), *Stochastic Processes and Filtering Theory*, Academic Press, San Diego, Calif.

Kalnay, E., et al. (1996), The NCEP/NCAR Reanalysis Project, *Bull. Am. Meteorol. Soc.*, *77*, 437–471.

Keppenne, C. L., and M. M. Rienecker (2002), Initial testing of a massively parallel ensemble Kalman filter with the Poseidon isopycnal ocean general circulation model, *Mon. Weather Rev.*, *130*, 2951–2965.

Kwok, R. (2002), Sea ice concentration estimates from satellite passive microwave radiometry and openings from SAR ice motion, *Geophys. Res. Lett.*, *29*(9), 1311, doi:10.1029/2002GL014787.

Large, W. C., J. C. McWilliams, and S. C. Doney (1994), Oceanic vertical mixing: A review and a model with a nonlocal boundary layer parameterization, *Rev. Geophys.*, *32*(4), 363–403.

Laxon, S. (2001), Simulated ice thickness from radar altimeter (task 4.1), in *The Quantification of the Importance of the Sea Ice Budget in the Climate System*, *Tech. Rep. 207*, Nansen Environ. and Remote Sens. Cent., Bergen, Norway.

Laxon, S., N. Peacock, and D. Smith (2003), High interannual variability of sea ice thickness in the Arctic region, *Nature*, *425*, 947–949, doi:10.1038/nature02050.

Levitus, S., and T. P. Boyer (1994), *World Ocean Atlas 1994*, vol. 4, *Temperature, NOAA Atlas NESDIS*, vol. 4, 129 pp., NOAA, Silver Spring, Md.

Levitus, S., R. Burgett, and T. P. Boyer (1994), *World Ocean Atlas 1994*, vol. 3 *Salinity, NOAA Atlas NESDIS*, vol. 3, 111 pp., NOAA, Silver Spring, Md.

Lindsay, R. W., and J. Zhang (2006), Assimilation of ice concentration in an ice-ocean model, *J. Atmos. Oceanic Technol.*, *23*, 742–749.

Lisæter, K. A., J. Rosanova, and G. Evensen (2003), Assimilation of ice concentration in a coupled ice-ocean model, using the ensemble Kalman filter, *Ocean Dyn.*, *53*, 368–388.

Marshall, J., and F. Schott (1999), Open-ocean convection: Observations, theory and models, *Rev. Geophys.*, *37*(1), 1–64.

Meier, W. N., J. A. Maslanik, and C. W. Fowler (2000), Error analysis and assimilation of remotely sensed ice motion within an Arctic sea ice model, *J. Geophys. Res.*, *105*(C2), 3339–3356.

Montgomery, R. B. (1938), Circulation in upper layers of southern North Atlantic deduced with use of isentropic analysis, *Pap. Phys. Oceanogr. Meteorol.*, *6*, 55 pp.

Peacock, N. R., and S. W. Laxon (2004), Sea surface height determination in the Arctic Ocean from ERS altimetry, *J. Geophys. Res.*, *109*, C07001, doi:10.1029/2001JC001026.

Pham, D. T. (2001), Stochastic methods for data assimilation in strongly nonlinear systems, *Mon. Weather Rev.*, *129*, 1194–1207.

Radionov, V. F., N. N. Bryazgin, and Y. I. Aleksandrov (1996), *The Snow Cover of the Arctic Basin*, Gidrometeoizdat, St. Petersburg, Russia.

Roach, A. T., K. Aagaard, and F. D. Carsey (1993), Coupled ice-ocean variability in the Greenland Sea, *Atmos. Ocean*, *31*, 319–337.

Rothrock, D. A., J. Zhang, and Y. Yu (2003), The arctic ice thickness anomaly of the 1990s: A consistent view from observations and models, *J. Geophys. Res.*, *108*(C3), 3083, doi:10.1029/2001JC001208.

Semtner, A. J., Jr. (1976), A model for the thermodynamic growth of sea ice in numerical investigations of climate, *J. Phys. Oceanogr.*, *6*, 379–389, 1976.

Teague, W. J., M. J. Carron, and P. J. Hogan (1990), A comparision between the generalized digital environmental model and Levitus climatologies, *J. Geophys. Res.*, *95*(C5), 7167–7183.

Visbeck, M., J. Fischer, and F. Schott (1995), Preconditioning the Greenland Sea for deep convection: Ice formation and ice drift, *J. Geophys. Res.*, *100*(C9), 18,489–18,502.

Whitaker, J. S., and T. M. Hamill (2002), Ensemble data assimilation without perturbed observations, *Mon. Weather Rev.*, *130*, 1913–1924.

Zhang, J., D. R. Thomas, D. A. Rothrock, R. W. Lindsay, and Y. Yu (2003), Assimilation of ice motion observations and comparisons with submarine thickness data, *J. Geophys. Res.*, *108*(C6), 3170, doi:10.1029/2001JC001041.

G. Evensen, Norsk Hydro, Oil & Energy Research Centre, PO Box 7190, N-5020 Bergen, Norway. (geir.evensen@nersc.no)

S. Laxon, Centre for Polar Observation and Modelling, University College London, London, UK. (swl@cpom.ucl.ac.uk)

K. A. Lisæter, Nansen Environmental and Remote Sensing Center, Thormøhlens gate 47, N-5006 Bergen, Norway. (knut.liseter@nersc.no)